INTEGRATED BLUETOOTH/IMT-E AND UWB PLANAR ANTENNA USING SCRLH RESONATOR TO REJECT WLAN AND WiMAX INTERFERENCES

Viet Hoang-The, Quyet Nguyen-Manh, Dong Hyun Lee, and Hyun Chang Park[*]

Division of Electronics and Electrical Engineering, Dongguk University-Seoul, 26, Pil-dong 3-ga, Chung-gu, Seoul 100-715, South Korea

Abstract—A novel printed monopole antenna covering 2.4–2.484 GHz (Bluetooth), 2.5–2.69 GHz (IMT-E) and 3.1–10.6 GHz (UWB) frequency bands is presented. The entire frequency bands are obtained by a modified U-shaped radiator and a modified ground plane. To prevent possible interference between UWB systems and other existing wireless systems such as WLAN and WiMAX, a SCRLH resonator structure is placed next to the feed line. Characteristics of the Bluetooth and IMT-E bands are further enhanced by two quarter-wavelength strips added on each side of the radiator. The proposed antenna can be easily printed on a 1.6-mm-thick FR4 substrate with dimensions of 30×41 mm^2. Simulation and experimental results show that the antenna yields an impedance bandwidth of 2.3–2.8 and 3–12 GHz with -10 dB reflection coefficient, except for the dual notched bands of 3.2–3.6 for WiMAX and 4.9–6.1 GHz for WLAN. The electrical characteristics in frequency and time domain show suitability of this antenna for use in UWB systems.

1. INTRODUCTION

Ultrawideband (UWB) technology combines attractive characteristics such as low cost, low complexity, and extremely high data rate for short ranges. A UWB antenna needs to possess desirable characteristics such as a broad bandwidth of 3.1–10.6 GHz [1], low profile, high radiation efficiency, and omnidirectional radiation patterns to realize the full potentials of UWB technology. Among the proposed UWB antennas,

printed monopole antennas have advantages of small size, ease of fabrication, low cost, and compatibility with the rest of the radio frequency (RF) front ends.

The design of UWB antennas still faces many challenges, including the problem of possible interferences between UWB systems and other existing wireless systems such as WiMAX at 3.3–3.6 GHz and WLAN at 5.15–5.825 GHz. To reject these interferences, various planar monopole UWB antennas with single or multiple band-notched characteristics have been presented [2–9]. Many of these antennas adopted several slots [2, 4–7] in the radiating patch and the ground plane, or parasitic strips [3] near the radiating patch to generate band-notched characteristics. However, the radiation pattern and the time-domain response of these antennas were negatively affected by the slot structures. The gain values were low at high frequencies [2, 3], or the fidelity factor was only less than 0.9 [4]. Other antennas used filter structures around the feed systems [8, 9]. In this case, the embedded filter structure increased the dimensions and the complexity of the final design. Recently, simplified composite right/left-handed (SCRLH) resonator structures have been implemented in various applications. Some of these structures show stop-band filtering behaviors, which can be used in the design of UWB antennas to reject undesired bands. In this paper, a simple SCRLH resonator structure is used to create stop-bands. Since the SCRLH resonator is placed next to the feed line of the proposed UWB antenna, the overall size of the antenna hardly changes. Moreover, dual band-notched characteristics can be easily created with only one SCRLH resonator, instead of multi EBG structures [10, 11] or multiple parasitic strips [12] with the same functionality, reducing the size and the complexity of the band-notch structures.

Meanwhile, the multi-function single-aperture approach has become an important part of the next-generation communication systems, requiring multi-service antenna technology. In [13], a printed Bluetooth and UWB antenna with dual band-notched functions was obtained using a microstrip-fed main patch and an electromagnetically coupled parasitic patch with arc-shaped strips. However, the final design of the antenna was quite complex. A printed super-wideband antenna was proposed in [14] with more than 25 : 1 impedance bandwidth, but radiation patterns in H-plane were omnidirectional only at low frequencies. A compact UWB antenna integrated with GSM/WCDMA/WLAN bands, as shown in [15], employed three folded Capacitive Loaded Line Resonators (CLLRs) to add three lower communication bands. However, the gains in these extra bands were low. An integrated Bluetooth and UWB antenna was also presented in [16], but the symmetry in the UWB antenna geometry was not

preserved as the Bluetooth element was integrated. In contrast, the UWB antenna proposed in this work integrates coverage of the Bluetooth and IMT-E bands [17] by modifying the resonator and the ground plane, while preserving the simple and symmetric antenna geometry. In addition, the proposed antenna exhibits positive peak gain values in the extra bands.

2. DESIGN AND ANALYSIS

This section describes the design process of the proposed antenna in three steps. First, a single antenna that covers 2.4–2.484 GHz (Bluetooth), 2.5–2.69 GHz (IMT-E) and 3.1–10.6 GHz (UWB) bands is designed. Then a SCRLH resonator structure is implemented to achieve rejections of WiMAX and WLAN frequency bands. Finally, two strip elements are integrated into the single antenna to improve the characteristics of the Bluetooth/IMT-E bands. Through simulations with the software Ansoft HFSS 13, the configuration of the final optimized antenna is obtained as shown in Figure 1. A modified U-shaped planar geometry is printed on a low cost FR4 substrate with a dielectric constant ε_r of 4.4, a loss tangent of 0.02, and a 50-Ω microstrip feed line. With substrate dimensions of $30 \times 41 \, \text{mm}^2$, this antenna can be easily integrated with a RF front-end. There is no ground metallization underneath the radiating element for proper operation.
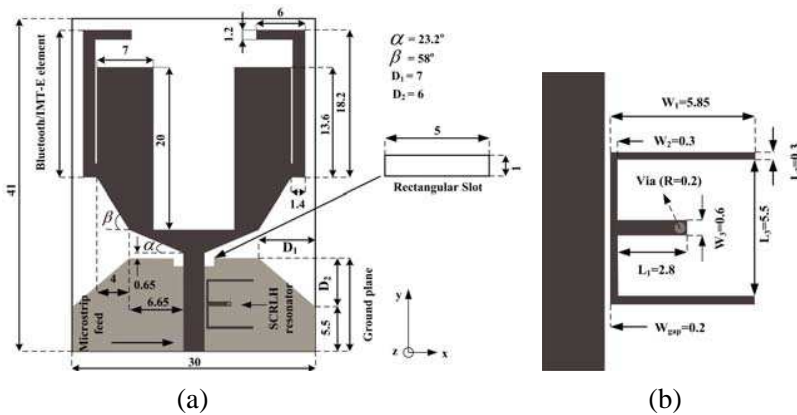

Figure 1. Geometry of (a) the proposed antenna, (b) the SCRLH resonator (unit: millimeter).

2.1. Design of the Single Antenna

In UWB communication systems, an antenna covering the whole operating frequency band is one of the necessary requirements. The proposed antenna consists of three parts: a modified U-shaped radiator, a microstrip feed line and a modified ground plane.

The antenna utilizes a U-shaped radiating element. Compared with a rectangular radiator, the current distribution on the ground plane is weaker for a U-shaped radiator. Therefore, influence of the ground plane on the impedance and radiation performance of the antenna can be reduced [18]. Geometric parameters of the radiating patch and the ground plane affect characteristics of the impedance match. Therefore, beveled edges were used in the design of U-shaped radiator and the ground plane to ensure good impedance match over broad frequency ranges [19]. For a simple rectangular ground plane $(D_1 = D_2 = 0)$, the reflection coefficient characteristics vary when
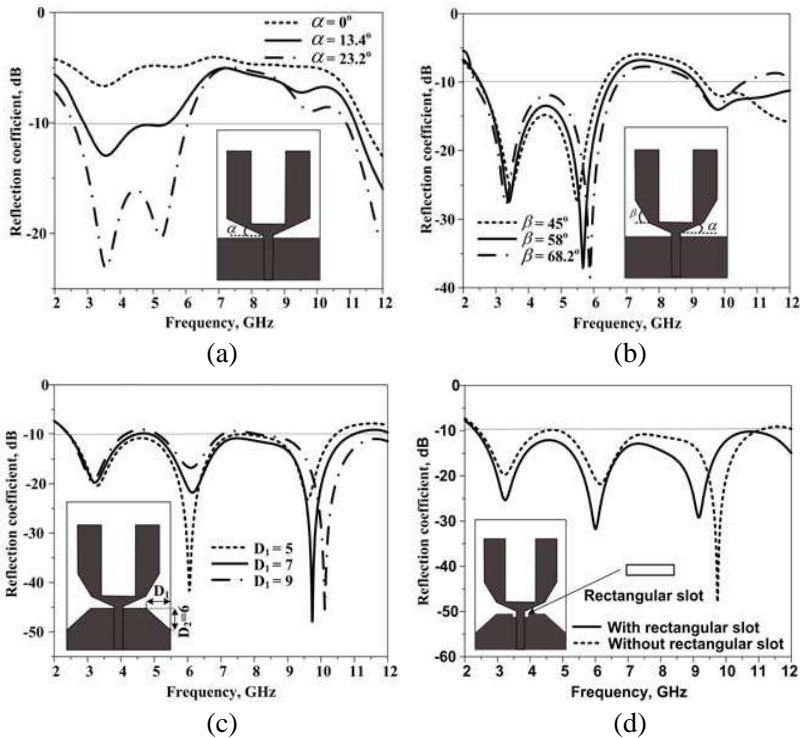
Figure 2. Simulated reflection coefficient of the antenna at various design stages.

the bevel angle of the modified U-shaped radiator changes. First, we varied the bevel angle α, and obtained best reflection coefficient characteristics when α was $23.2°$. However, the impedance of the radiating patch and the input impedance became mismatched at the frequency band from $6\,\text{GHz}$ to $11\,\text{GHz}$, resulting in the reflection coefficient greater than $-10\,\text{dB}$ as shown in Figure 2(a). Next, fixing α at $23.2°$, the second bevel angle β was changed to further improve the bandwidth of the antenna. Figure 2(b) shows that the overall characteristics improved most with $\beta = 58°$. However, it was still not efficient enough to achieve the middle cut-off frequency of the antenna, as the reflection coefficient was still greater than $-10\,\text{dB}$ from $6.5\,\text{GHz}$ to $9\,\text{GHz}$. Therefore, the rectangular ground plane structure was also beveled to improve the reflection coefficient over the desired band. As shown in Figure 2(c), with the value of $D_1 = 7\,\text{mm}$ and $D_2 = 6\,\text{mm}$, the reflection coefficient became less than $-10\,\text{dB}$ from $2.4\,\text{GHz}$ to $11\,\text{GHz}$. The reflection coefficient was improved even further when a rectangular slot was cut in the beveled ground plane near the feed point, as is evident in Figure 2(d). The rectangular slot also acts as a smooth transition from one resonant mode to another, providing well-matched wideband characteristics that cover Bluetooth, IMT-E and UWB bands. Optimized values of α, β, D_1, D_2 and dimensions of the rectangular slot are shown in Figure 1(a).
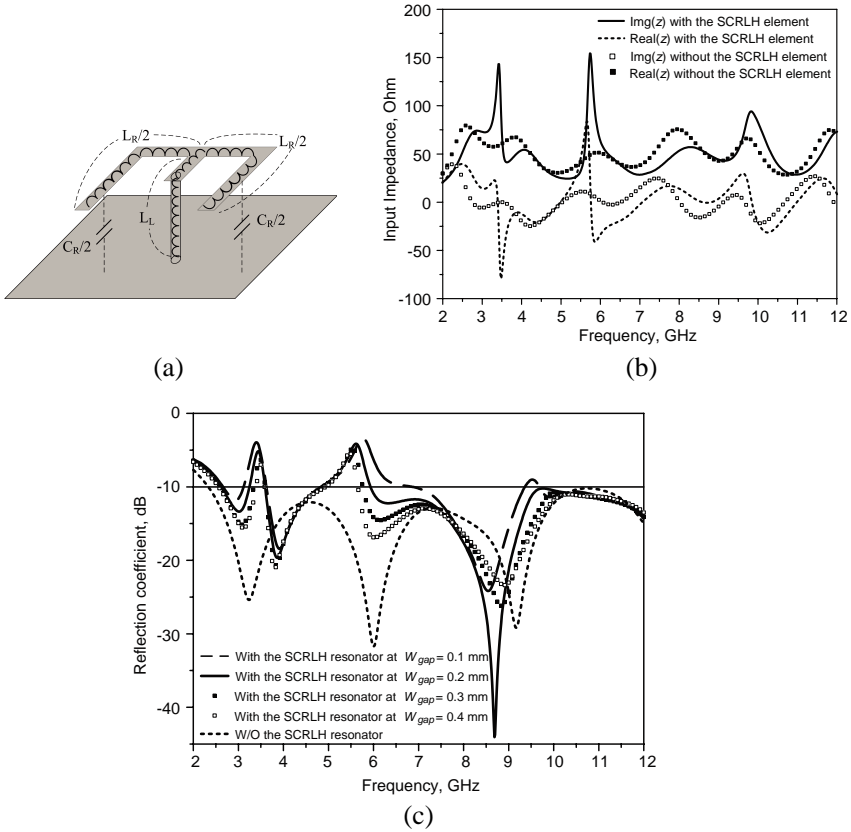
2.2. Design of the SCRLH Resonator

Dual-band rejection covering the 3.3–$3.6\,\text{GHz}$ and 5.15–$5.85\,\text{GHz}$ is desired in order to prevent possible interferences with the WiMAX and WLAN systems. The rejection was achieved using a SCRLH resonator structure as detailed in Figure 1(b). The SCRLH resonator can be designed to achieve dual cut-off based on high/low-impedance short-line elements and grounded stubs [20–22], with the resonant frequencies given approximately by the expressions,

$$\omega_1 = \frac{1}{\sqrt{L_L C_R}}, \quad \omega_2 = \frac{\sqrt{1 + 4L_L/L_R}}{\sqrt{L_L C_R}} \tag{1}$$

where L_R and C_R are the series inductance and the shunt capacitance of the short-line elements, respectively. The shunt inductance L_L comes from the metalized via hole connecting the E-shaped patch to the ground, as shown in Figure 3(a).

As the SCRLH element is placed close to the feed line, the resonator is strongly coupled to it and captures and stores most of the input energy at its resonance frequencies, effectively creating a dual band-notch filter as shown in Figure 3(b). It can be seen that large impedance mismatch occurs at $3.3\,\text{GHz}$ and $5.65\,\text{GHz}$,

(a)

(b)

(c)

Figure 3. (a) Equivalent circuit of the SCRLH resonator, (b) simulated input impedance of the antenna with and without the SCRLH resonator, and (c) simulated reflection coefficient of the antenna at various W_{gap} values.

corresponding to the notch-band positions. Figure 3(c) shows that the optimized separation between the feed line and the SCRLH element is $W_{gap} = 0.2$ mm. The excited surface current distributions of the SCRLH element simulated using the software HFSS at 3.3 and 5.65 GHz are presented in Figure 4. In Figure 4(a), a large surface current distribution is observed along the metalized via hole and the connecting edge of the E-shaped patch at 3.3 GHz. On the other hand, at 5.65 GHz, surface current is concentrated along the E-shaped patch and weak at the metalized via hole, as seen in Figure 4(b). This shows that the shunt inductance L_L is important in determining the
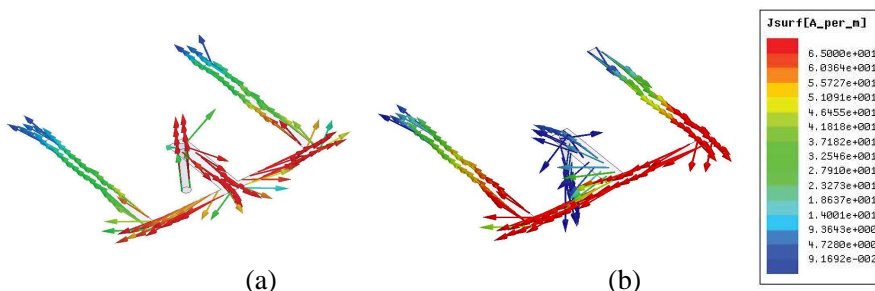
Figure 4. Simulated surface current distributions of the SCRLH resonator at (a) 3.3 GHz and (b) 5.65 GHz.

lower resonance frequency, whereas the series inductance L_R affects the higher resonance frequency. It was also observed that the notch-band frequencies could be adjusted by changing the resonator dimensions. Both notched bands moved up in frequency as the parameter L_2 was decreased. Only the upper notched band moved up as L_3 was decreased, while only the lower notched band moved up as L_1 was decreased. Optimum values of the resonator dimensions are shown in Figure 1(b). However, due to the influence of the SCRLH resonator structure, the antenna no longer covers the Bluetooth and IMT-E frequency bands comfortably, requiring further improvement for these bands.

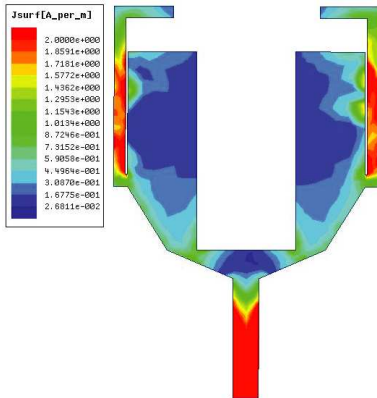## 2.3. Design of the Bluetooth/IMT-E Element

To boost the Bluetooth and IMT-E frequency bands, two quarter-wavelength strips are attached to the single antenna. The strips are added at the symmetric positions of minimum current to ensure a minimal coupling between the two elements [16]. The length of each strip is about a quarter-wavelength at the operating frequency $f = 2.5$ GHz. The guided wavelength is given by,

$$\lambda_g = \frac{\lambda}{\sqrt{\varepsilon_{reff}}}, \quad \varepsilon_{reff} = \frac{\varepsilon_r + 1}{2} \tag{2}$$

where λ is the free space wavelength and ε_r is the dielectric constant of the substrate. As shown in Figure 5, characteristics of the Bluetooth/IMT-E band have greatly improved. The excited surface current distributions of the Bluetooth/IMT-E element at 2.4 GHz are presented in Figure 6. It can be seen that the surface current is concentrated at the lower strips.
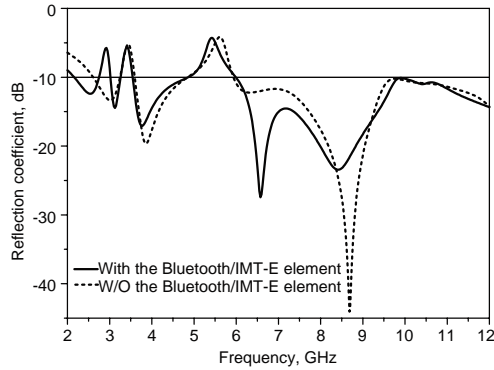
Figure 5. Simulated reflection coefficient of the antenna with and without the Bluetooth/IMT-E element.


Figure 6. Simulated surface current distributions of the Bluetooth/IMT-E element at 2.4 GHz.
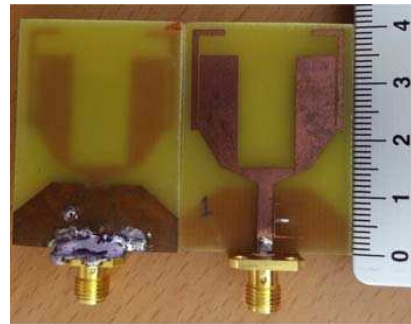
Figure 7. Photograph of the fabricated antenna.

3. RESULTS AND DISCUSSIONS

The monopole antenna was successfully fabricated as shown in Figure 7. The impedance bandwidth was measured using an Agilent 8719A network analyzer. Measured and simulated reflection coefficients show good agreement as observed in Figure 8. The antenna exhibits a $-10\,$dB bandwidth of 500 MHz for the Bluetooth/IMT-E band from 2.2 GHz to 2.7 GHz and a bandwidth from 3 GHz to 11 GHz for the UWB band. It also exhibits two designed notched bands of 3.2–
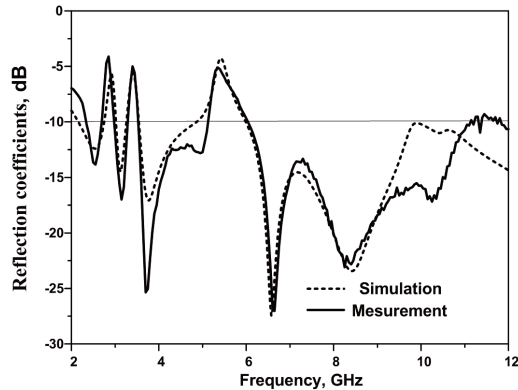
Figure 8. Measured and simulated reflection coefficient of the final antenna structure.

3.6 GHz (WiMAX) and 4.9–6.1 GHz (WLAN) with only one SCRLH resonator structure. The slight differences between the simulation and the measurement results are attributed to the inserted SMA connector at the input port and the changes in dimensions during fabrication.

Antenna radiation patterns were measured in an anechoic chamber. Normalized radiation patterns of the antenna with the SCRLH structure are simulated and measured across the *E*- (*yz*-) and the *H*- (*xz*-) planes at 2.4, 3, 3.4, 5.8, 6.4 and 9 GHz as presented in Figures 9(a)–9(f), respectively. The simulated and measured results show good agreement. Near omnidirectional patterns in the *H*-plane and dipole-like radiation patterns in the *E*-plane are observed at pass-band frequencies. It is also observed that the SCRLH structure does not affect the radiation patterns in pass-band frequencies as shown in Figures 9(a), 9(b), 9(e) and 9(f). On the other hand, the radiation patterns are distorted and less omnidirectional with reduced radiation intensity at the notch-band frequencies of 3.4 and 5.8 GHz as shown in Figures 9(c) and 9(d).

The calculated average radiation efficiency by HFSS over the pass-band frequencies is about 90%. Figure 10 shows calculated and measured maximum gains of the antenna as a function of frequency. Two sharp reductions at two notched bands clearly confirm the signal-rejecting capability of the proposed antenna. Using only one SCRLH resonator to create dual band-notched characteristics, this antenna occupies less space and can be fabricated more easily compared with the antennas in [10, 11] with similar functionality. The peak gain values of the proposed antenna, especially at high frequency, are higher than
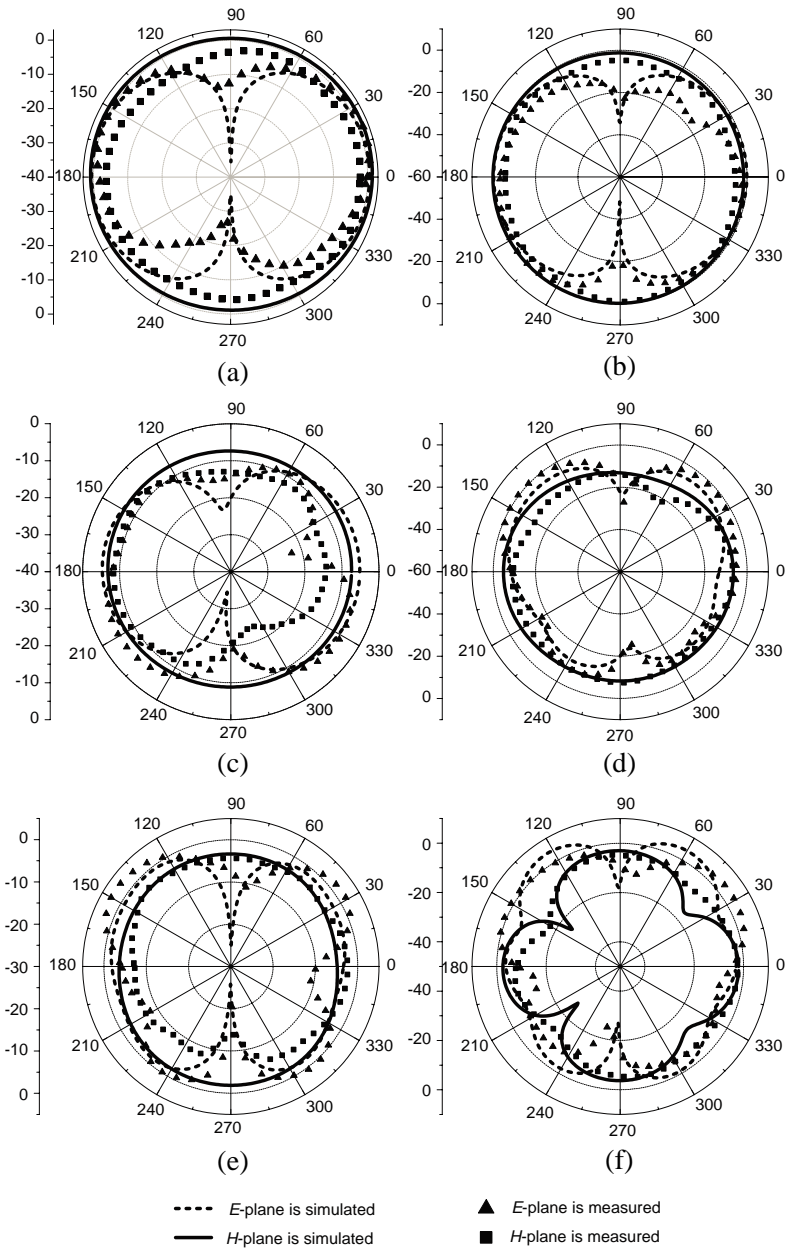
Figure 9. Simulated and measured radiation pattern in the *H*- and the *E*-planes at (a) 2.4, (b) 3, (c) 3.4, (d) 5.8, (e) 6.4, and (f) 9 GHz.
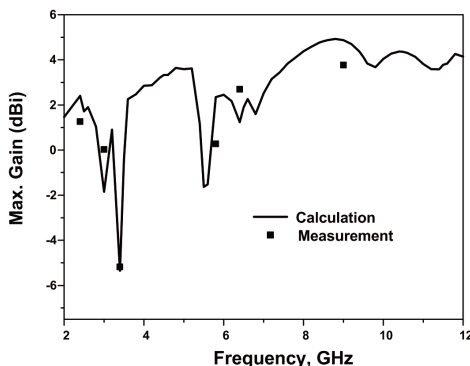
Figure 10. Calculated and measured maximum gain of the antenna.

those of the antennas in [2, 3]. Moreover, the proposed antenna exhibits positive peak gain values in the extra bands whereas the antenna in [15] shows negative peak gain values in these bands.

In order to assess the signal fidelity of this antenna, time-domain responses were examined. Fifth-derivative of the Gaussian pulse [23, 24] defined by the following equation was chosen as the input pulse signal to the transmitting antenna without the SCRLH resonator.

$$s_1(t) = A\left(-\frac{(t-t_0)^5}{\sigma^{11}} + \frac{10(t-t_0)^3}{\sigma^9} - \frac{15(t-t_0)^3}{\sigma^7}\right)\frac{e^{-(t-t_0)^2/2\sigma^2}}{\sqrt{2\pi}} \quad (3)$$

Here, A is a constant chosen to meet the FCC emission level, t_0 the time shift chosen to be $0.5\,\mathrm{ns}$ for all pulses, and σ controls the pulse width, chosen to be $51\,\mathrm{ps}$ to ensure that the shape of the spectrum complies with the spectral mask. The input signal and its Fourier transform are shown in Figures 11(a) and 11(b). The distance between the transmitting and the receiving antennas is set to be $100\,\mathrm{mm}$ to ensure far-field operation. It is assumed that both antennas have the same orientation and are placed face-to-face. The signal at the $50\,\Omega$ output terminal of the receiving antennas with and without the SCRLH resonator, along with its Fourier transform, is shown in Figures 11(c) and 11(d).

The distortion between the transmitted pulse and the received pulse is assessed by the fidelity factor. The fidelity factor F is the maximum correlation coefficient between the signal $s_2(t)$ at the output terminal of the receiving antenna and the input signal $s_1(t)$ at the transmitting antenna as determined by the following equation,

$$F = \max_{\Gamma}\left\{\frac{\int s_1(t)s_2(t-\Gamma)dt}{\sqrt{s_1^2(t)dt}\sqrt{s_2^2(t)dt}}\right\} \quad (4)$$

(a)

(b)

(c)

(d)
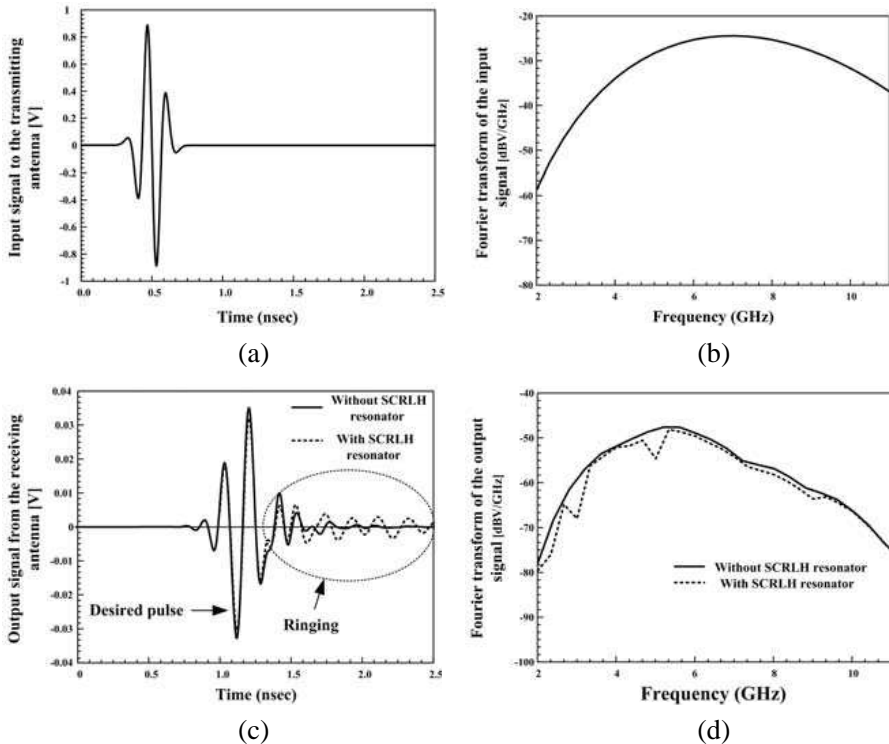
Figure 11. (a) UWB input signal to the transmitting antenna, (b) Fourier transform of the input signal, (c) output signal from the receiving antenna, and (d) Fourier transform of the output signal.

where Γ is a delay varied to make the numerator in (4) a maximum value. The values of the fidelity factor obtained with and without the SCRLH resonator structure are 0.912 and 0.940. Therefore, although the output signal at the terminal of the dual band-notched antenna is somewhat more distorted than that of the antenna without the notched bands, mostly in the ringing portion, the proposed antenna can still manage to receive good signals in the wide frequency range as the degradation in the fidelity factor from 0.940 to 0.912 is less than 3% only. These fidelity factors are higher compared with those of the antennas in [4, 7].

4. CONCLUSION

A novel integrated Bluetooth/IMT-E and UWB printed monopole antenna with dual band-notched characteristics is proposed, fabricated

and characterized. The dual-band characteristics were achieved by a modified U-shaped radiator and a modified ground plane, and further improved by adding two quarter-wavelength strips at each side of the antenna. The dual band-notched characteristics to reject possible interferences with WLAN or WiMAX systems were easily obtained with only one SCRLH resonator structure placed next to the feed line. The fabricated antenna showed good agreement between measured and simulated results. Time-domain analysis of the demonstrated antenna showed high signal fidelity even with the band-notched characteristics.

ACKNOWLEDGMENT

REFERENCES

1. First Report and Order in the Matter of Revision of Part 15 of the Commission Rules Regarding Ultra-wideband Transmission Systems, Released by Federal Communications Commission (FCC), ET-Docket 98-153, 2002.

2. Zhou, D., S. Gao, F. Zhu, R. A. Abd-Alhameed, and J. D. Xu, "A simple and compact planar ultra wide-band antenna with single or dual band-notched characteristics," *Progress In Electromagnetics Research*, Vol. 123, 47–65, 2012.

3. Zhu, F., S. Gao, A. T. S. Ho, C. H. See, R. A. Abd-Alhameed, J. Li, and J. Xu, "Design and analysis of planar ultra-wide band antenna with dual band notched function," *Progress In Electromagnetics Research*, Vol. 127, 523–536, 2012.

4. Ghatak, R., B. Biswas, A. Karmakar, and D. R. Poddar, "A circular fractal UWB antenna based on descartes circle theorem with band rejection capability," *Progress In Electromagnetics Research C*, Vol. 37, 235–248, 2013.

5. Nguyen, D. T., D. H. Lee, and H. C. Park, "Small planar coplanar-waveguide-fed dual band-notched monopole ultra-wideband antenna," *Microwave Opt. Technol. Lett.*, Vol. 53, No. 4, 920–924, 2011.

6. Nguyen, D. T., D. H. Lee, and H. C. Park, "Very compact printed triple band-notched UWB antenna with quarter-wavelength slots," *IEEE Antennas Wireless Propag. Lett.*, Vol. 11, 411–414, 2012.

7. Wu, Z. H., F. Wei, X. W. Shi, and W. T. Li, "A compact quad band-notched UWB monopole antenna loaded one lateral L-shaped slot," *Progress In Electromagnetics Research*, Vol. 139, 303–315, 2013.

8. Djaiz, A., M. Nedil, M. A. Habib, and T. A. Denidni, "Design of a new UWB-integrated antenna filter with a rejected WLAN band at 5.8 GHz," *Microwave Opt. Technol. Lett.*, Vol. 53, No. 6, 1298–1302, 2011.

9. Panda, J. R. and R. S. Kshetrimayum, "A 3.4/5.5 dual-band notched UWB printed monopole antenna with two open-circuited stubs in the microstrip feedline," *Microwave Opt. Technol. Lett.*, Vol. 53, No. 12, 2973–2978, 2011.

10. Son, T. V. and D. N. Chien, "Dual band-notched UWB antenna based on electromagnetic band gap structures," *REV Journal on Electronics and Communications*, Vol. 1, 130–136, 2011.

11. Peng, L. and C. Ruan, "Design and time-domain analysis of compact multi-band-notched UWB antennas with EBG structures," *Progress In Electromagnetics Research B*, Vol. 47, 339–357, 2013.

12. Liu, X., Y. Yin, P. Liu, J. Wang, and B. Xu, "A CPW-fed dual band-notched UWB antenna with a pair of bended dual-L-shape parasitic branches," *Progress In Electromagnetics Research*, Vol. 136, 623–634, 2013.

13. Ren, F. C., F. S. Zang, J. H. Bao, Y. C. Jiao, and L. Zhou, "Printed Bluetooth and UWB antenna with dual band-notched functions," *Progress In Electromagnetics Research Letters*, Vol. 26, 39–48, 2011.

14. Dong, Y., W. Hong, L. Liu, Y. Zhang, and Z. Kuai, "Performance analysis of a printed super-wideband antenna," *Microwave Opt. Technol. Lett.*, Vol. 51, No. 4, 949–956, 2009.

15. Li, G., H. Zhai, T. Li, X. Ma, and C. Liang, "Design of a compact UWB antenna integrated with GSM/WCDMA/WLAN bands," *Progress In Electromagnetics Research*, Vol. 136, 409–419, 2013.

16. Yildirim, B. S., B. A. Cetiner, G. Roqueta, and L. Jofre, "Intergrated Bluetooth and UWB antenna," *IEEE Antennas Wireless Propag. Lett.*, Vol. 8, 149–152, 2009.

17. Hu, C. L., D. L. Huang, H. L. Kuo, C. F. Yang, C. L. Liao, and S. T. Lin, "Compact multibranch inverted-F antenna to be embedded in a laptop computer for LTE/WWAN/IMT-E applications," *IEEE Antennas Wireless Propag. Lett.*, Vol. 9, 834–841, 2009.

18. Chen, Z. N., T. S. P. See, and X. Qing, "Small printed ultrawideband antenna with reduced ground plane effect," *IEEE Trans. Antennas Propag.*, Vol. 55, No. 2, 383–388, 2007.

19. Chu, Q. X. and Y. Y. Yang, "3.5/5.5 GHz dual band-notch ultra-wideband antenna," *Electron. Lett.*, Vol. 44, No. 3, 172–174, 2008.

20. Han, W. and Y. Feng, "Ultra-wideband bandpass filter using simplified left-handed transmission line structure," *Microwave Opt. Technol. Lett.*, Vol. 50, No. 11, 2758–2762, 2008.

21. Gong, J. Q. and Q. X. Chu, "Miniaturized microstrip bandpass filter using coupled SCRLH zeroth-order resonators," *Microwave Opt. Technol. Lett.*, Vol. 51, No. 12, 2985–2989, 2009.

22. Wei, F., Q. Y. Wu, X. W. Shi, and L. Chen, "Compact UWB bandpass filter with dual notched bands based on SCRLH resonator," *IEEE Microwave Wireless Compon. Lett.*, Vol. 21, No. 1, 28–30, 2011.

23. Elmansouri, M. A. and D. S. Filipovic, "Pulse distortion and mitigation thereof in spiral antenna-based UWB communication systems," *IEEE Trans. Antennas Propag.*, Vol. 59, No. 10, 3863–3871, 2011.

24. Lizzi, L., G. Oliveri, and A. Massa, "A time-domain approach to the synthesis of UWB antenna systems," *Progress In Electromagnetics Research*, Vol. 122, 557–575, 2012.